JOURNAL OF MATERIALS SCIENCE 15 (1980) 1109–1123

A model for the toughness of epoxy-rubber particulate composites

S. KUNZ-DOUGLASS
Sandia Laboratories, Albuquerque, New Mexico, USA

P. W. R. BEAUMONT, M. F. ASHBY
Department of Engineering, University of Cambridge, Trumpington Street, Cambridge, UK

Epoxy resins are toughened significantly by a dispersion of rubber precipitates. Microscopic examinations of propagating cracks in epoxy–rubber composites reveal that the brittle epoxy matrix cracks, leaving ligaments of rubber attached to the two crack surfaces. The rubber particles are stretched as the crack opens and fail by tearing at large, critical extensions. This fracture mechanism is the basis of a new analytical model for toughening. An increase in toughness (ΔG_{IC}) of the composite is identified with the amount of elastic energy stored in the rubber during stretching which is dissipated irreversibly (e.g. as heat) when the particles fail. The model predicts the failure strain of the particles in terms of their size. It also relates the toughness increase to the volume fraction and tearing energy of the rubber particles. Direct measurements of the tearing strains of rubber particles, and toughness data obtained from epoxy–rubber composites, are in good agreement with the model. The particle-stretching model provides a quantitative explanation, in contribution to existing qualitative theories, for the toughening of epoxy–rubber composites.

1. Introduction

A number of theories have been proposed to explain the toughening effect of rubber particles on brittle polymers. Early theories of the rubber particles acting as energy-absorbers [1] or crack-stoppers [2] in high-impact polystyrene, for example, were later discounted. Observations of microcracking [3], later redescribed as crazing [4], induced by the stress-concentrating particles, led to emphasis on the role of the matrix in toughening. Matrix-controlled processes such as crazing [4], shear yielding [5] and, more recently, combined multiple-crazing and craze-termination [6] are considered the dominant mechanisms of energy absorption in toughening polymers. These mechanisms are generally consistent with the yield behaviour of thermoplastic polymers; in rubber-modified cross-linked thermosets (e.g. epoxy, polyester), however, only isolated and largely speculative observations of crazes or shear bands have been reported [7–10]. A further disadvantage in applying existing toughness theories to rubber-toughened epoxy is their lack of quantitative models by which each mechanism's contribution to the fracture energy can be evaluated and predicted.

This paper describes the development of an analytical toughening model based upon microscopic observations of crack propagation in epoxy–rubber composites. Rubber particles bridge the matrix crack; as the crack advances they are stretched to large strains and fail by tearing. The model gives a quantitative prediction for the toughening contribution (ΔG_{IC}) of the rubber particles in terms of their volume fraction and tearing energy. Direct measurements of observed microfracture processes, and toughness data from epoxy–rubber composites, are used to test the model.

0022–2461/80/051109–15$03.50/0

TABLE I Properties of CTBN rubbers

	A (CTBN 1300 X 13)	B (CTBN 1300 X 8)	C (CTBN 130 X 15)	D (CTB 2000 X 162)
Acrylonitrile content (%)	27	18	10	0
Molecular weight	3400	3500	3600	4000
Carboxyl (%)	2.40	2.37	2.47	1.9
Functionality	1.85	1.85	1.9	2.01
Specific gravity at 25° C	0.960	0.948	0.924	0.907
EPHR*	0.059	0.053	0.057	0.043
	0.056	0.052		

* Equivalents per hundred of rubber.

2. Composition and morphology of composites

2.1. Epoxy resin

The epoxy resin was a diglycidyl ether of bisphenol A (DGEBA), having a mean molecular weight of 300 and an epoxide content of 5.2 eq kg^{-1}. The curing agent was 4,4′-diaminodiphenylmethane (DDM), an aromatic amine. It is a crystalline solid with a molecular weight of 198.8, a functionality of 4 and a melting point of 100° C.

Castings of epoxy resin were made from 100 parts by weight (pbw) resin and 27 pbw hardener. The melted curing agent was mixed with a portion of pre-heated resin at 100° C before adding the remaining room temperature resin. Mechanical stirring of the mixture was followed by degassing in a vacuum chamber and casting the resin into a steel mould pre-heated to 70° C. A cure cycle of 2 h at 80° C, 1 h at 120° C and 2 h at 180° C was used.

2.2. Epoxy–rubber composites

Four kinds of carboxyl-terminated butadiene-acrylonitrile (CTBN) liquid rubber were used with the DGEBA resin. The molecular weights ranged between 3400 and 4000, and the acrylonitrile contents varied between 0% and 27%. Table I summarizes the properties of the rubbers [10].

TABLE II Composition and morphology of composites

Composite type	CTBN rubber	W_R (%)	V_R (%)	V_P (%)	$\bar{d}$ STD (X 10^6 m)	l (X 10^6 m)	l^*
I	A	4.95	6.06	7.17	0.17 ± 0.1	–	–
		10.10	12.22	14.42	0.25 ± 0.2	–	–
		15.04	17.99	20.83	0.29 ± 0.2	–	–
	B	5.06	6.27	8.77	1.84 ± 2.0	8.20	2.72
		10.15	12.42	16.93	3.15 ± 2.0	8.97	0.64
		15.10	18.25	29.14	4.03 ± 3.0	8.64	
	C	5.19	6.59	14.25	4.49 ± 20.0	16.19	2.40
		10.14	12.69	30.39	7.69 ± 20.0	16.08	–
		15.19	18.75	38.04	6.05 ± 10.0	10.26	–
	D	4.97	6.42	10.71	4.09 ± 50.0	22.15	5.79
		10.17	12.93	25.30	9.71 ± 60.0	31.42	–
		15.22	19.06	42.90	38.42 ± 40.0	69.03	–
II	A	5.25	6.43	8.13	0.18 ± 0.1	–	–
		10.02	12.13	12.81	0.26 ± 0.2	–	–
		15.59	18.63	18.50	0.42 ± 0.3	–	–
	B	5.25	6.50	6.42	1.86 ± 1.3	8.02	3.43
		10.02	12.26	13.91	2.36 ± 1.3	6.90	1.09
		15.56	18.78	28.94	3.33 ± 3.1	8.30	–
	C	5.25	6.66	7.77	3.60 ± 4.2	19.81	7.35
		10.02	13.26	18.10	8.40 ± 9.5	29.4	1.10
		15.57	19.19	30.18	21.10 ± 22.4	57.8	–

Epoxy–CTBN composites were fabricated with concentrations of 5%, 10% and 15% (by weight) of each rubber. These concentration levels were obtained by mixing 100 pbw epoxy resin and 27 pbw hardener with 7, 14.5 and 23 pbw rubber, respectively. The resin and rubber were mixed using two methods: simple reaction and pre-reaction.

2.2.1. Simple reaction (type I composites)

In this case, the CTBN rubber was warmed to 70° C and then stirred into the epoxy/hardener mixture. After degassing, the mixture was cast into a pre-heated mould. The cure cycle was similar to that used for pure epoxy resin.

2.2.2. Pre-reaction (type II composites)

100 pbw resin were mixed initially with 80 pbw CTBN rubber and heated to 150° C for 4 h. The resin–rubber blend was then diluted with the appropriate stoichiometric amounts of resin and curing agent to give the desired concentration of rubber in the composite. Subsequent stages of fabrication were similar to those followed for the simple reaction method.

The four CTBN rubbers used are designated A, B, C and D, in order of decreasing acrylonitrile content. Type I composites were made with rubbers A, B, C and D, and type II composites were limited to rubbers A, B, and C. For ease of future reference, each epoxy–CTBN composite is classified according to its method of fabrication and by the elastomer it contains, e.g. II-B.

Table II lists the composites together with the weight fraction (W_R) and volume fraction (V_R) of rubber, volume fraction particles (V_P) and average particle diameter ($\bar{d}$). V_R is calculated from the weight fraction and density of rubber used in fabrication. V_P is obtained directly, using a Quantimet, from the area fraction of particles measured from micrographs of polished composite sections [11]. In types I and II composites, the average size of particle varied between 0.2 and 40 μm, depending upon the type and weight fraction of rubber. Volume fractions of rubber between 0.06 and 0.18 resulted in volume fractions of rubber precipitates between 0.07 and 0.43. Increasing the amount of acrylonitrile, i.e. from 0%, 10%, 18% to 27%, decreased the size of the rubber particles and produced a range of overlapping sizes between 0.07 and 100 μm, approximately [11].

The precipitated rubber phase is thought to be a mixture of epoxy–CTBN co-polymers and cross-linked epoxy [12]. Furthermore, because phase separation is never complete, some of the elastomer remains in solution with the epoxy matrix [13].

3. Role of rubber particles during fracture

A crack was propagated in samples of the composites by driving a wedge into a pre-cut notch. The region at and near the crack tip was studied by optical microscopy. Fig. 1 shows typical observations: stretched rubber particles span the crack, acting like little springs between its faces; as the crack is wedged further open, first the larger, then the smaller particles fail.

A sequence of photographs of a single particle is shown in Fig. 2. The particle of initial diameter, d, contracts under strain, forming a "neck" between the crack faces (a). Slight opening of the crack stretches the particle (b) and leads to a decrease in the neck diameter and an increase in its radius of curvature. Further straining causes rupture of the outermost fibres of rubber visible on the left edge of the neck in (c). This process corresponds to stable tearing of the rubber. The tear extends at a constant crack opening (i.e. fixed displacement), progressively reducing the neck diameter, and subsequently becomes arrested (d).

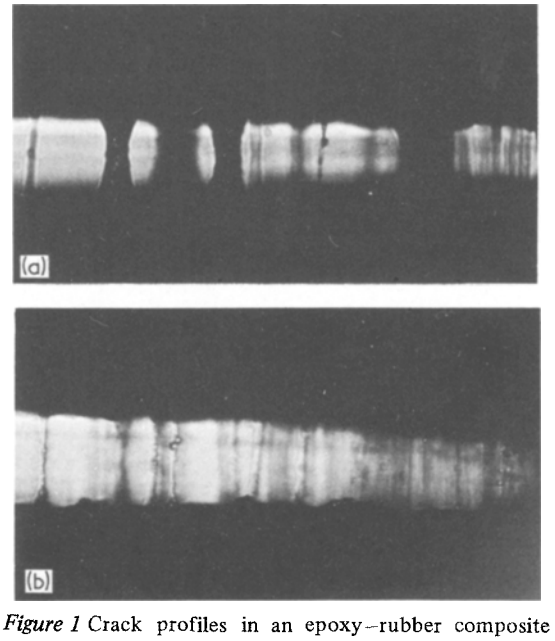

Figure 1 Crack profiles in an epoxy–rubber composite showing rubber particles between 3 and 30 μm diameter being stretched in (a); failure of the largest particles occurs as the crack opening is increased in (b).

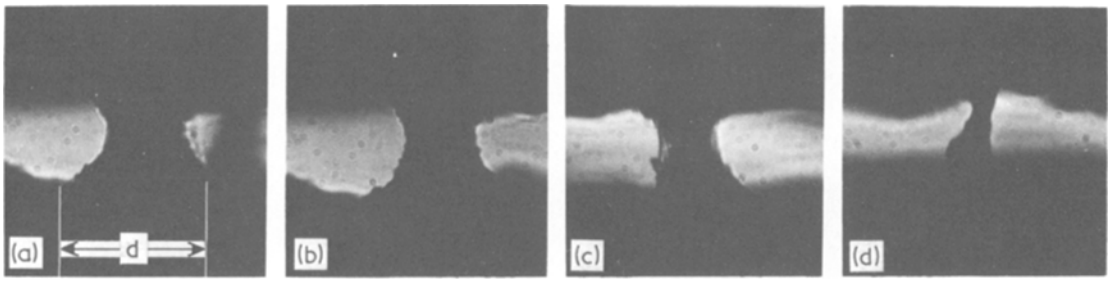

Figure 2 Failure sequence of a particle stretched between the surfaces of a matrix crack showing the propagation of a tear through the rubber at a fixed crack opening ($d \simeq 100\,\mu m$).

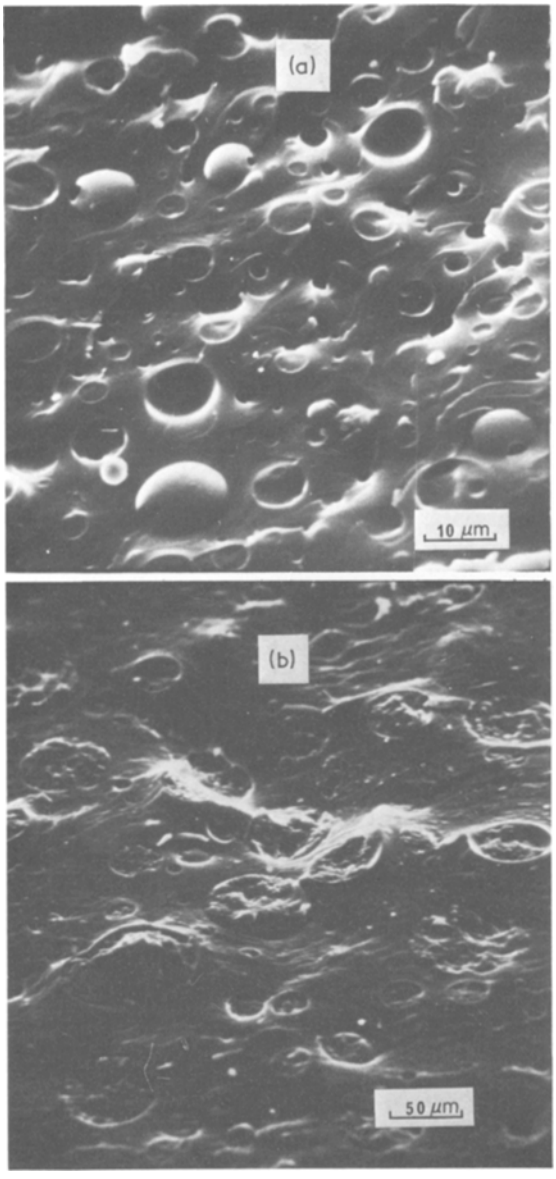

Figure 3 Typical fracture surfaces of (a) type II-B and (b) type II-C epoxy–rubber composites showing rubber particles protruding from the plane of the matrix and cavities from which the particles were torn.

A decrease in the apparent diameter of the particle is observed between (a) and (d) as the torn rubber retracts towards the crack faces. Tear propagation continues and leads to complete rupture of the particle only when the crack opening is increased.

Typical fracture surfaces in Fig. 3 reveal rubber particles protruding above the plane of the matrix as well as cavities out of which rubber has been torn. This suggests that tearing of the rubber occurs within the hemispherical region of the particles. Photographs of the same surfaces shown at higher magnifications in Fig. 4 indicate that the depth to which a tear followed a curved path through the rubber varies inversely with the particle size: the embedded remnants of small particles ($d \simeq 2$ to $12\,\mu m$) in (a) are nearly spherical in shape, whereas those of larger ones ($d \simeq 30$ to $60\,\mu m$) reflect a more shallow and flat tearing path. Furthermore, the particles appear to be well bonded to the matrix. Flaws in the rubber at which tearing may have been initiated are visible along the particle–matrix interfaces in Fig. 4a and b.

4. Development of a model

4.1. The toughness increase in terms of the tearing strain of the rubber

The observations of crack propagation in epoxy resin containing dispersed rubber particles are summarized schematically in Fig. 5. A notched sample is loaded in tension (a); at the fracture stress of the brittle matrix, a crack extends (b), by-passing the rubbery particles without penetrating them; as the crack propagates (c), the particles bonded to the matrix are stretched between the opening crack and fail when they reach a critical, large extension.

Consider the region behind the tip of the propagating crack shown in Fig. 6. A rubber particle lying in the fracture plane is stretched

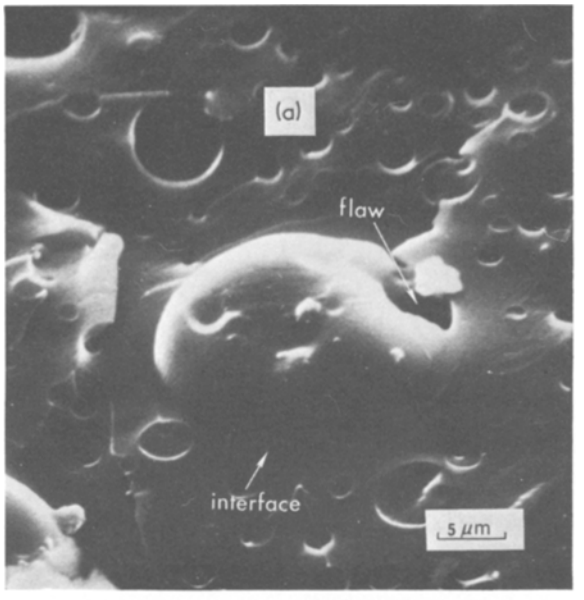

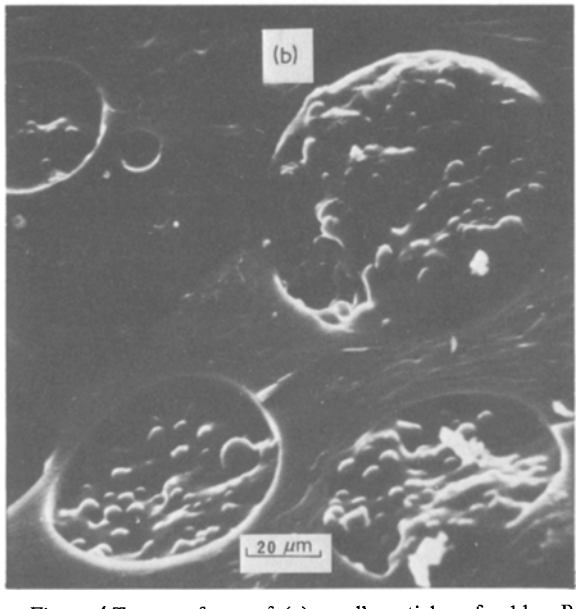

Figure 4 Torn surfaces of (a) small particles of rubber B and (b) large particles of rubber C. The particles are well bonded to the matrix and contain flaws along the particle–matrix interface at which tearing can initiate.

between the opening crack faces and stores an amount of elastic energy per unit volume, W_0, given by

$$W_0 = \int_1^{\lambda} \sigma \, d\lambda \qquad (1)$$

where λ is the extension ratio ($d\lambda = dl/l_0$ where l_0 is the initial length and dl is the increase in length). The stress–extension relation for rubber in simple tension is [14]

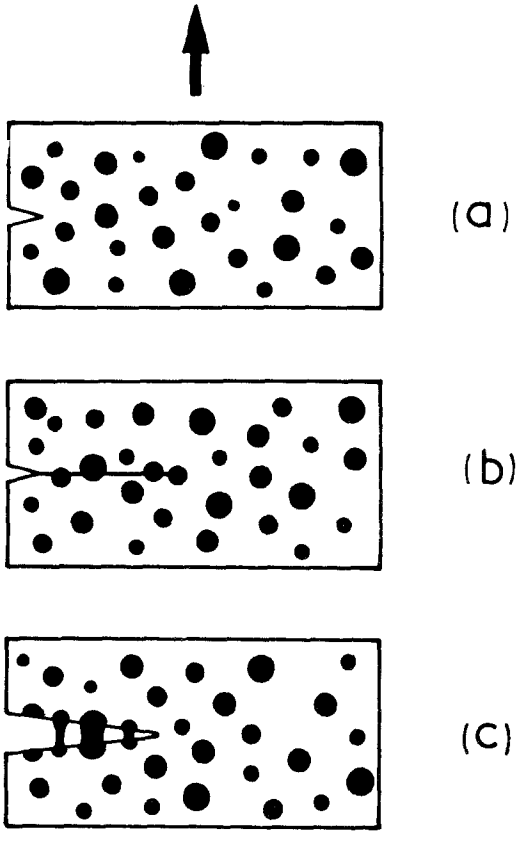

Figure 5 Schematic diagram showing the stages of crack propagation in epoxy resin containing a dispersion of rubber particles.

$$\sigma = G\left(\lambda - \frac{1}{\lambda^2}\right). \qquad (2)$$

Near the breaking strain, λ_f, the shear modulus, G, increases as the molecular chains are drawn into alignment and reach their maximum extensibility. The strain energy density of the rubber when extended to large strains is therefore determined

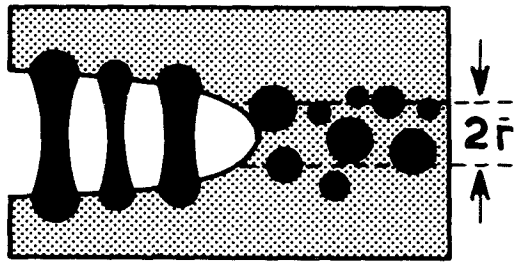

Figure 6 Schematic representation of the region near the tip of a crack in an epoxy–rubber composite showing stretching of the rubber particles between the matrix fracture surfaces.

by an average or effective shear modulus, $\bar{G}$, and (from Equations 1 and 2) is given by

$$W_0 = \tfrac{1}{2}\bar{G}\left(\lambda^2 + \frac{2}{\lambda} - 3\right). \quad (3)$$

The work done in stretching a particle of volume V to failure then becomes

$$W_p = \tfrac{1}{2}\bar{G}\left(\lambda_f^2 + \frac{2}{\lambda_f} - 3\right)V. \quad (4)$$

If this energy is dissipated when the particle fails, then an increase in toughness, ΔG_{IC}, due to the particles can be identified by

$$\Delta G_{IC} = W_p N_A, \quad (5)$$

where N_A is the number of particles per unit area of fracture surface:

$$N_A = \frac{3}{2}\frac{V_P}{\pi \bar{r}^2}, \quad (6)$$

for a dispersion of particles of mean radius $\bar{r}$ (see, for example, [15]). Hence the toughness increase becomes

$$\Delta G_{IC} = \bar{G}\left(\lambda_f^2 + \frac{2}{\lambda_f} - 3\right)V_P \bar{r}. \quad (7)$$

Its magnitude can be evaluated only if λ_f, the tearing strain of the rubber is known.

4.2. Tearing strain of the rubber

When the crack faces of one of these composites is opened, a "forest" of rubber ligaments can be seen at the crack tip and up to 2 mm behind it. Fig. 1 shows typical profiles of cracks spanned by rubber particles. The particles ($d \simeq 3$ to $30\,\mu$m) are stretched to lengths greater than three times their diameters and exert a spring-like resistance to crack opening. As the crack opening increases, the rubber ligaments furthest from the crack tip rupture successively.

In general, the tensile failure of rubber does not involve the simultaneous breaking of all molecules crossing the fracture plane [14, 16]. Instead, the molecular chains rupture successively by the propagation of a tear, originating at a flaw. The model for particle failure, illustrated in Fig. 7, is based on the above observations. Tearing is assumed to initiate in a stretched particle at an existing flaw at the rubber–matrix interface (see Figs. 4 and 7a). Opening the crack (Fig. 7b) stretches the tip of the tear and the tearing site appears blunt. Bonding of the rubber to the matrix is assumed to constrain the direction of tearing. Thus, at fixed displacement of the crack faces (Fig. 7c) the tear penetrates the hemispherical region of the particle, following the contour of the particle–matrix interface. Closure of the crack faces (Fig. 7d) reveals the resulting curved path of the tear. Tearing increases the effective height of rubber being stretched and hence relaxes the strain at a fixed crack opening. This is consistent with the observation that continuous tearing of a particle require a continuously increasing crack opening.

An idealized epoxy–rubber composite was

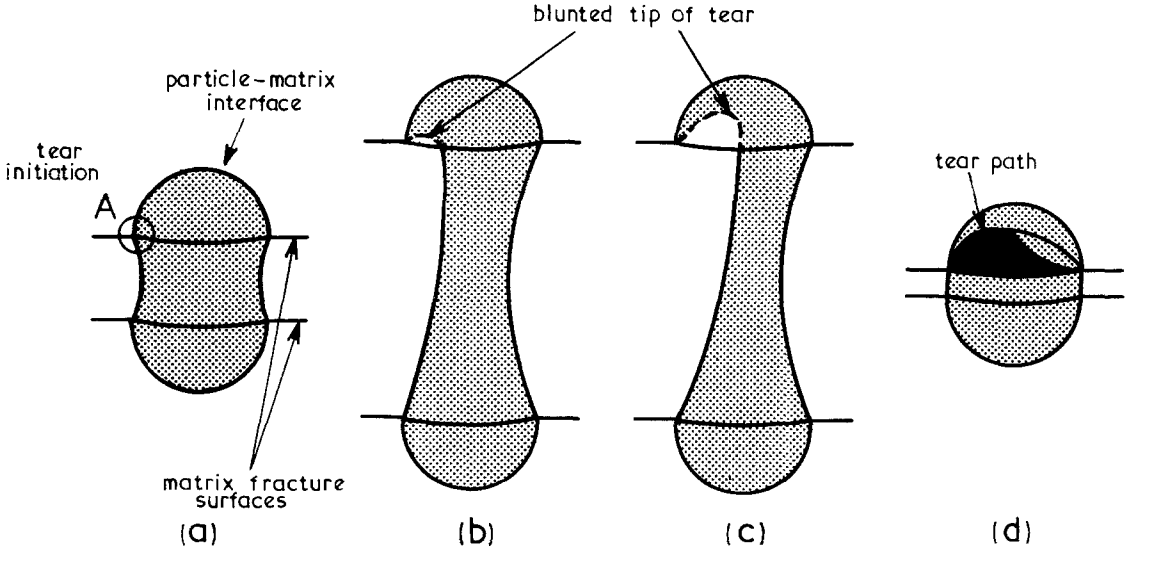

Figure 7 Schematic representation of tearing of a rubber particle. Closure of the matrix crack (d) shows the tearing path within the hemispherical region of the particle.

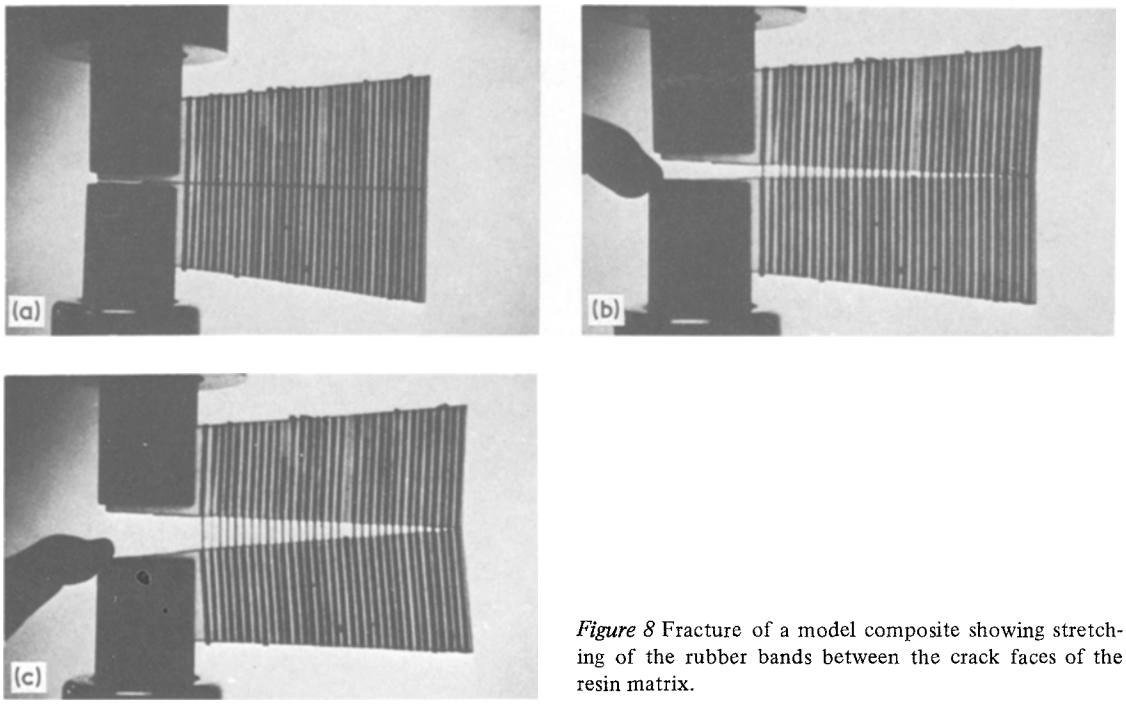

Figure 8 Fracture of a model composite showing stretching of the rubber bands between the crack faces of the resin matrix.

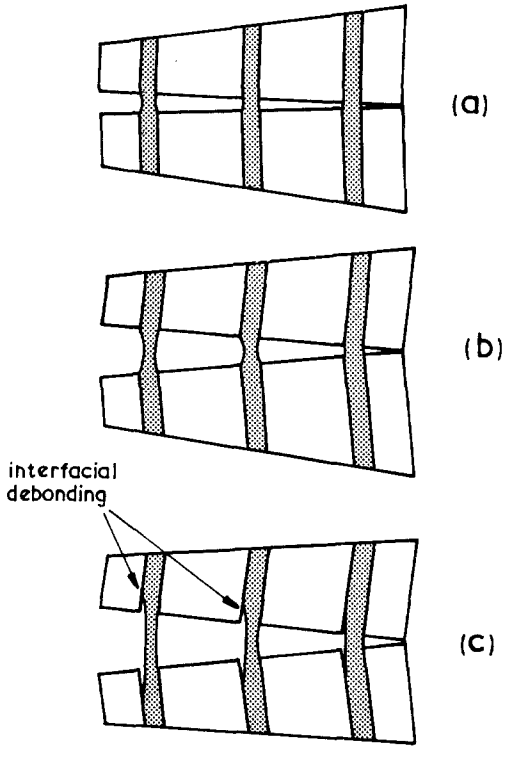

Figure 9 Schematic diagram of fracture processes in a model composite showing stretching of rubber bands between the matrix fracture surfaces (a, b) and debonding from the matrix (c).

constructed to simulate the failure mechanism of the rubber particles. Rubber bands (1.6 mm × 0.8 mm) were aligned across a mould, in a single row and at regular intervals (3.5 and 7 mm). After casting and curing the epoxy resin, tapered double-cantilever beam specimens were machined from the plates and tested in tension as shown in Fig. 8. The failure processes observed are illustrated schematically in Fig. 9. A crack propagated catastrophically through the matrix (a), circumventing the rubber bands which remained firmly bonded to the resin. Opening the crack (b) stretched the rubber bands between the fracture surfaces of the matrix. As the crack was opened further (c), the rubber bands began to debond from the resin at the surfaces of the matrix crack. The rubber bands progressively "peeled" away from the resin by the propagation of a crack along the rubber–matrix interface.

Consider the initial stage of failure of the idealized composite. A single rubber band is isolated and represented as a cylinder which is stretched as the crack faces separate (Fig. 10a and b). When the rubber debonds from the matrix over a distance dl and at a fixed separation of the crack faces (Fig. 10c) the strain energy in it decreases. From Equation 4 the change in elastic

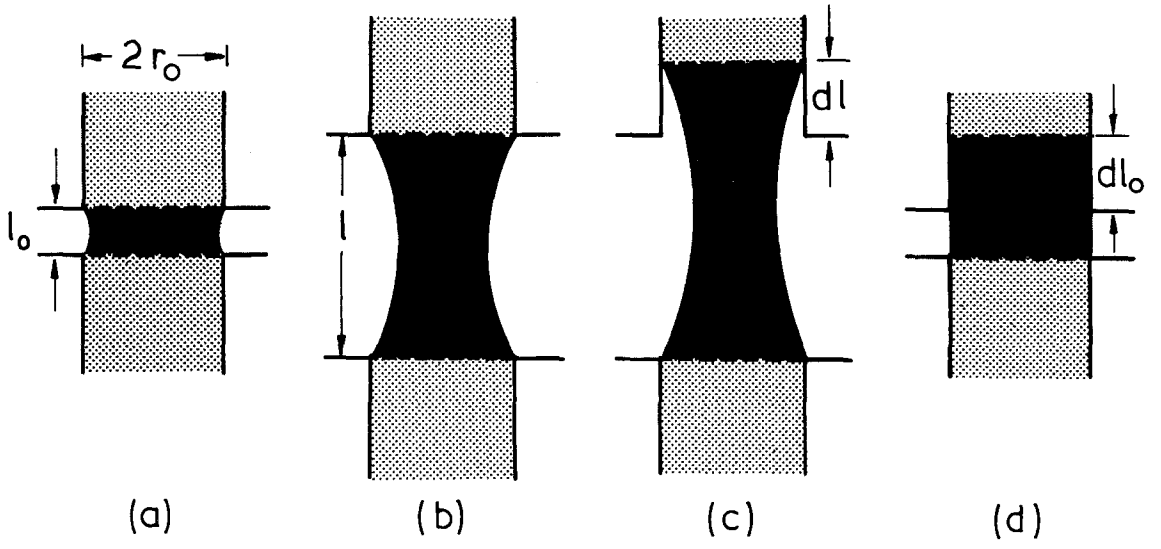

Figure 10 Schematic representation of stretching and debonding of rubber in an idealised epoxy-rubber composite.

energy is

$$dW = \tfrac{1}{2}\bar{G}\left[\left(\lambda^2 + \frac{2}{\lambda} - 3\right)dV + V\left(2\lambda - \frac{2}{\lambda^2}\right)d\lambda\right]. \quad (8)$$

The first term in the brackets describes the effect of the increase in length and hence volume of the strained region; the second describes the effect of the decrease in the extension ratio. Writing

$$dV = A_0\, dl_0$$

$$d\lambda = -\lambda\frac{dl_0}{l_0},$$

where l_0 is the length (the unstretched length of the segment of the rubber band which stretches when the crack opens) and A_0 is the initial cross-sectional area of the band, the strain-energy release rate in the band is then

$$\frac{dW}{dl_0} = -\tfrac{1}{2}\bar{G}\left[\lambda^2 - \frac{4}{\lambda} + 3\right]A_0. \quad (9)$$

For interfacial debonding to occur, the amount of elastic energy released by the rubber must exceed or equal the energy absorbed in the debonding process. This condition is expressed by

$$\frac{dW}{dl_0} + \frac{dS}{dl_0} \leqslant 0, \quad (10)$$

where S is the energy associated with newly formed interfacial surface. The increase in S is given by

$$dS = \Gamma_i \cdot dA, \quad (11)$$

where Γ_i is the energy per unit area of interface required to debond rubber from the matrix, and $dA = 2\pi r_0 \cdot dl_0$ (Fig. 10d) is the area of newly debonded interface. Equation 10 now becomes

$$-\tfrac{1}{2}\bar{G}\left[\lambda^2 - \frac{4}{\lambda} + 3\right]\pi r_0^2 + 2\pi r_0 \cdot \Gamma_i \leqslant 0. \quad (12)$$

A similar expression applies to the initiation of a tearing failure of rubber particles in a composite. In this instance the rubber–matrix interface is assumed to be sufficiently strong so that the rubber tears near the interface rather than debonds. Replacing the debonding energy, Γ_i, by the tear energy of the rubber Γ_t, and the band radius r_0 by the particle radius $\bar{r}$, and rearranging, leads to:

$$\lambda_t^2 - \frac{4}{\lambda_t} + 3 = \frac{4\Gamma_t}{\bar{G}\bar{r}}. \quad (13)$$

This expression defines the extension ratio, λ_t, at which a rubber particle will start to tear.

4.3. Predictions of the model

The experiments described in Section 3 showed that the rubber particles fail by tearing. The quantity λ_f in Equation 7 is therefore identified with the extension ratio at which particles tear (λ_t), given by Equation 13. Dividing the first equation by the second leads to

$$\Delta G_{IC} = \left[\frac{\lambda_t^2 + (2/\lambda_t) - 3}{\lambda_t^2 - (4/\lambda_t) + 3}\right]4\Gamma_t \cdot V_p. \quad (14)$$

The term in brackets can be expressed using partial fractions, giving:

$$\Delta G_{IC} = \left[1 - \frac{6}{\lambda_t^2 + \lambda_t + 4}\right] 4\Gamma_t \cdot V_P. \quad (15)$$

The term in brackets assumes a value between 0.2 and 0.75 for $1.5 \leqslant \lambda_t \leqslant 4$, but converges towards 1 when $\lambda_t \geqslant 4$. Thus, the value of ΔG_{IC} predicted by Equation 15 can be approximated by

$$\Delta G_{IC} = 4\Gamma_t V_P \quad (\lambda_t > 4). \quad (16)$$

The tearing strain (Equation 13) depends on particle size, becoming larger the smaller the particles. However, the overall contribution of the particles to the toughness is much less sensitive to $\bar{r}$: when the tearing strain is small, there is a dependence of ΔG_{IC} on $\bar{r}$ (through λ_t, see Equation 15); but when the strain is large, it disappears (Equation 16), and the toughness increment depends only on the volume fraction and tear energy of the rubber itself.

If toughness of the composite as a whole is expressed using a simple rule of mixtures

$$G_{IC} = G_{IC}^{E}(1 - V_P) + \Delta G_{IC} \quad (17)$$

(where the superscript E refers to the epoxy matrix), then the limiting toughness when the tearing strain is large ($\lambda_t > 4$) is

$$G_{IC} = G_{IC}^{E}(1 - V_P) + 4\Gamma_t V_P. \quad (18)$$

The toughness decreases as the tearing strain of the particles decreases ($\lambda_t \leqslant 4$).

5. Comparison of model with experiment

5.1. Dependence of λ_t on particle size

The model for particle stretching and tearing (Equation 13) predicts that the failure strain of a particle should depend inversely on the particle size. Fig. 1 illustrates this behaviour: a matrix crack (a) is spanned by particles ranging between 3 and 30 μm diameter; as the crack opens (b), the larger particles fail while the smaller ones continue to extend.

Direct measurements of the failure strains of rubber particles were obtained for a range of particle sizes; photographs were taken of rubber particles at the first sign of tearing during opening of the matrix crack. Fig. 11 defines the parameters involved. The gauge length, l_0, is approximated by

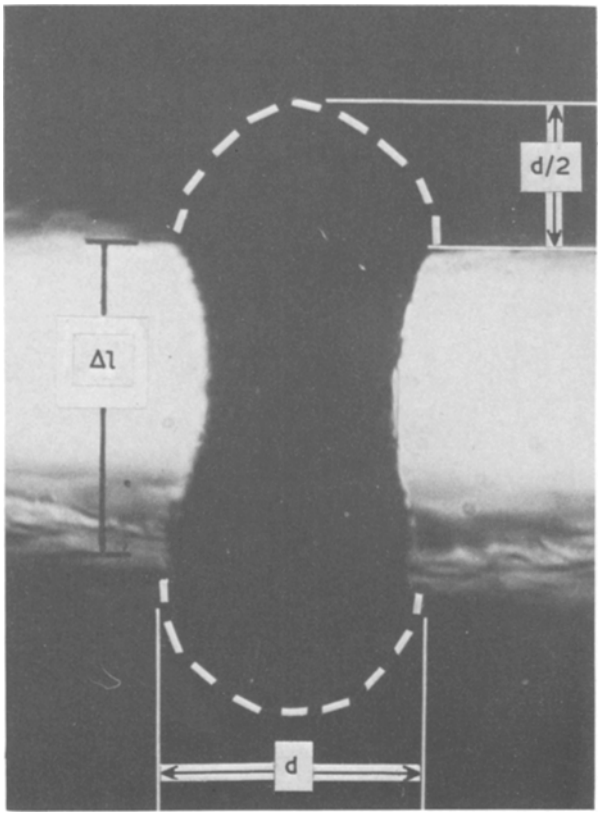

Figure 11 Photograph of a stretched rubber particle sho-ing the dimensions measured to calculate the tearing strain from Equation 19.

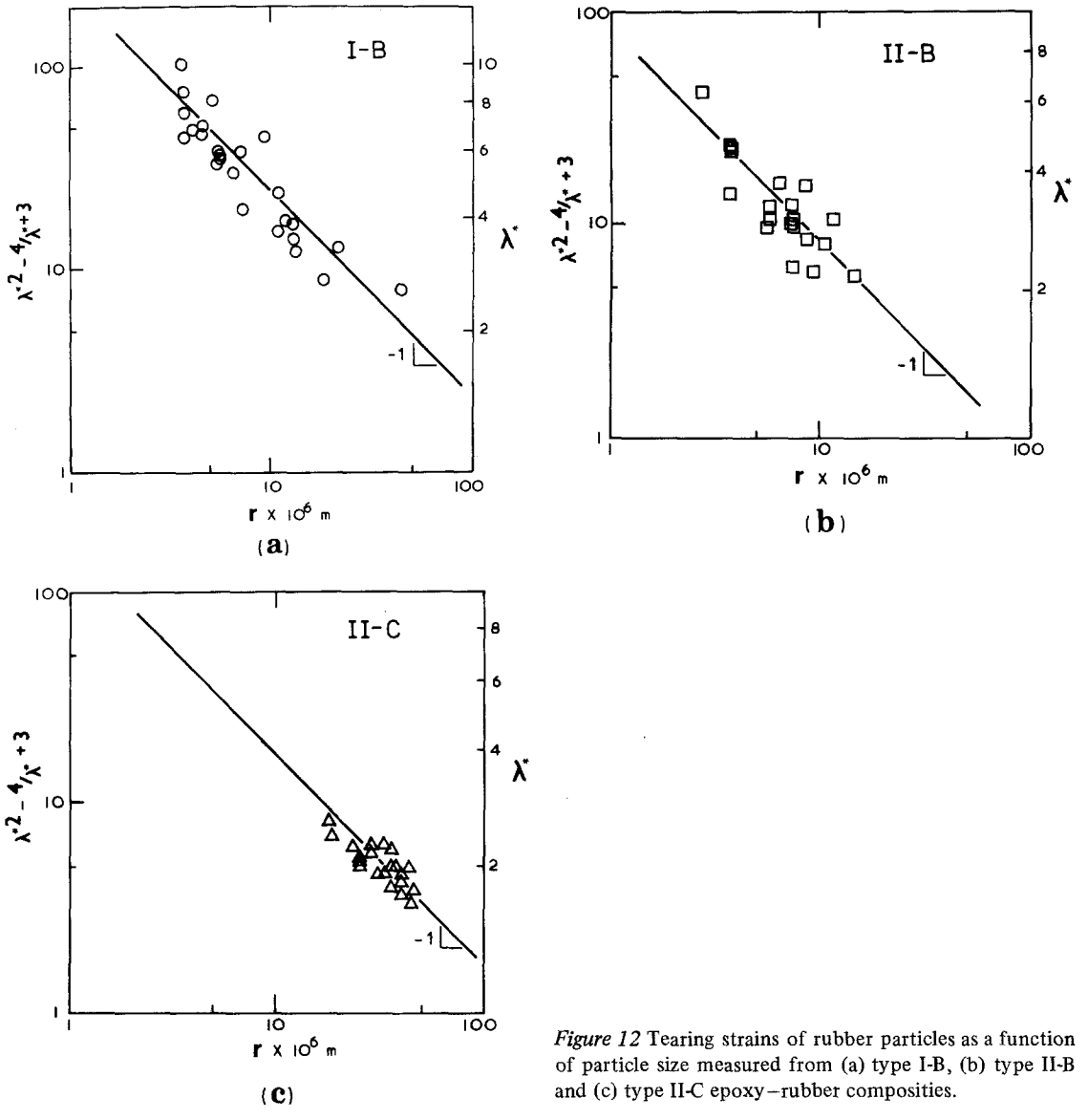

Figure 12 Tearing strains of rubber particles as a function of particle size measured from (a) type I-B, (b) type II-B and (c) type II-C epoxy–rubber composites.

setting it equal to the particle diameter, d. The experimental extension ratio at failure, λ^*, is then determined from

$$\lambda^* = \frac{l}{d} = \frac{\Delta l + d}{d} \tag{19}$$

where Δl is the measured length of rubber stretched between the crack faces (Fig. 11) when tearing starts.

Values of λ^*, were measured for particles ranging between 2 and 50 μm in diameter from composites fabricated with rubbers B and C (types I–B, II–B and II–C). Measurements of Δl and d from particles at the onset of tearing were used to calculate λ^* according to Equation 19. The corresponding values of $\lambda^{*2} - (4/\lambda^*) + 3$ are plotted logarithmically in Fig. 12a, b and c for composites I–B, II–B and II–C, respectively.

Each of the three sets of experimental data is well described by a straight line. Equation 13 written in logarithmic form as

$$\ln\left[\lambda_t^2 - \frac{4}{\lambda_t} + 3\right] = -\ln r + \ln\frac{4\Gamma_t}{\bar{G}} \tag{20}$$

predicts a gradient equal to -1. A least squares regression on the data in Fig. 12a and b gave slope values of -0.98 and -0.95 respectively. A linear regression could not be used for the data in Fig. 12c due to the limited range of r values of which λ^*

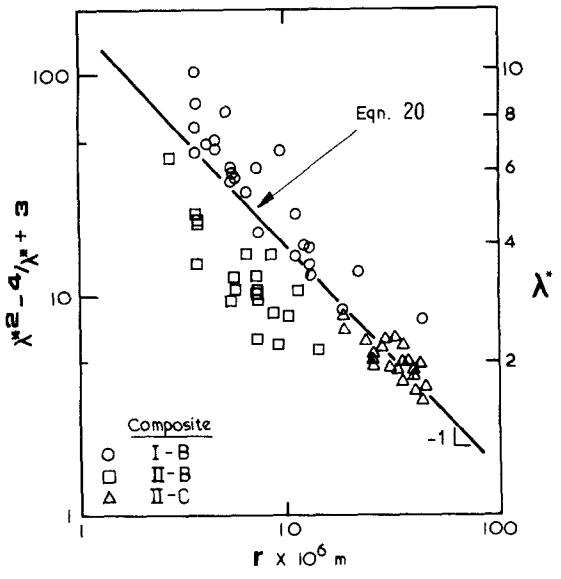

Figure 13 Cumulative plot of tearing strains of tubber particles measured from expoy–rubber composites as a function of the particle size showing comparison with theory.

was measured; nevertheless the data can be represented by a line of best fit with a slope of -1.

All three sets of experimental data are plotted together in Fig. 13. The small, systematic vertical displacements between the sets is believed to reflect differences in the values of Γ_t and $\bar{G}$ for the different rubbers (see below). The figures, taken together, indicate that the particle size dependence of λ^* is well accounted for by the model (Equation 13).

5.2. Dependence of toughness of particle volume fraction

The toughening model, expressed in the form of Equation 15, predicts a linear dependence of ΔG_{IC} on V_P with a gradient which is directly proportional to the tear energy of the particles. A double torsion test was used to measure G_{IC} of the epoxy–rubber composites as well as of the pure epoxy resin, G_{IC}^E. The quantity ΔG_{IC} was then calculated using Equation 17, where the measured value of G_{IC}^E was $300\,J\,m^{-2}$. Values of ΔG_{IC} are plotted in Fig. 14 as a function of V_P and show the predicted linear dependence.

5.3. Tearing energy of the rubber particles

Apparent tear energies of the particles can be calculated directly from the slopes of the exper-

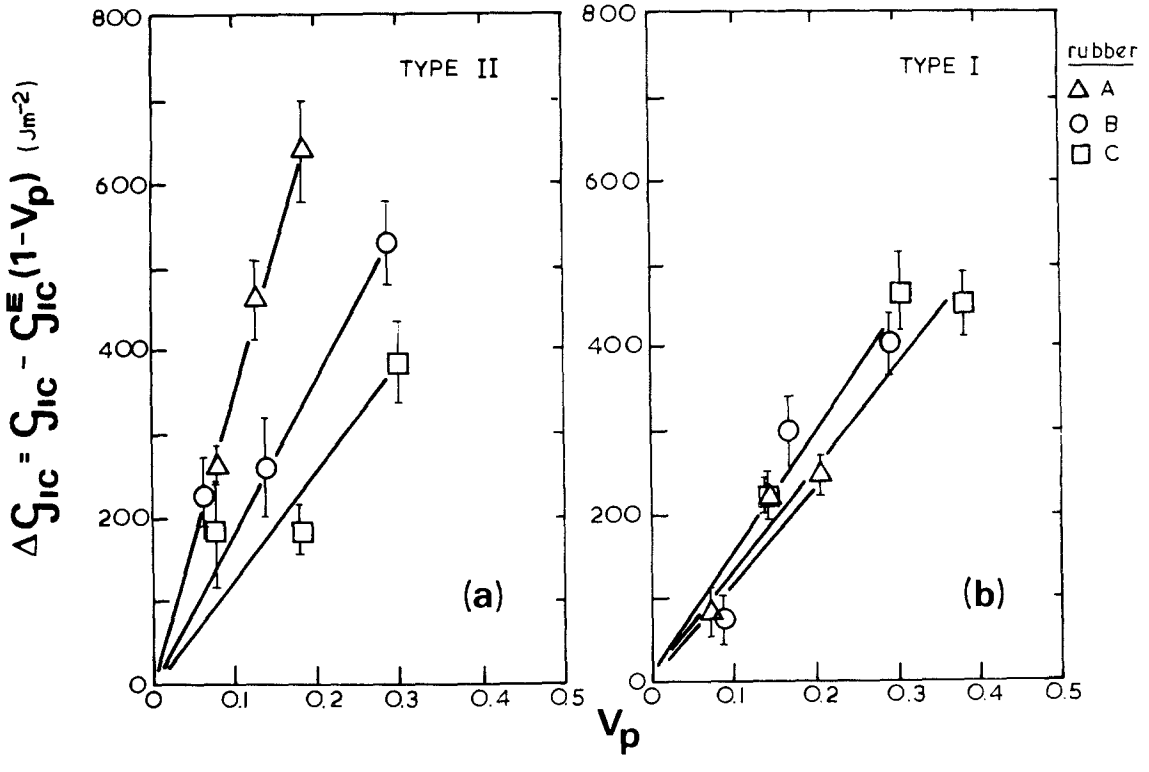

Figure 14 Increase in toughness as a function of particle voluem fraction for (a) type II and (b) type I expoy–rubber composites.

TABLE III

Rubber	Γ_t (J m^{-2})	
	Composite I	Composite II
A	320 ± 50	880 ± 100
B	370 ± 50	460 ± 50
C	640 ± 130	640 ± 130

imental lines in Fig. 14. The results are presented in Table III. Rubbers A and B produce particles between approximately 0.1 and 20 μm. These particles have tearing extension ratios (λ_t) greater than 4 (see Fig. 13) and Γ_t is therefore given by the ratio $\Delta G_{IC}/4V_P$ (Equation 16). By contrast, rubber C gives rise to particles greater than $\sim 20\,\mu$m diameter which fail at extension ratios less than 4. The corresponding tear energies are therefore calculated using Equation 15.

The tearing energy of the rubber particles can be evaluated also from the experimental plots in Fig. 12, using Equation 13 expressed in the form

$$\frac{4\Gamma_t}{\bar{G}} = \left[\lambda_t^2 - \frac{4}{\lambda_t} + 3\right] r.$$

The quantity $4\Gamma_t/\bar{G}$, calculated from $\lambda^{*2} - (4/\lambda^*) + 3$ at a value of $r = 10\,\mu$m, is equal to 2.4 ($\pm$ 1.0) $\times 10^{-4}$ m, 0.8 ($\pm$ 0.3) $\times 10^{-4}$ m and 1.7 ($\pm$ 0.4) $\times 10^{-4}$ m for materials I–B, II–B and II–C, respectively. Γ_t is estimated by assuming an effective large-strain shear modulus, $\bar{G}$, of the order of $3G$ [19]. The shear modulus of rubbers, having compositions similar to those of the particles, is typically about 1.0 MN m^{-2} [11, 14], giving $\bar{G} \approx 3$ MN m^{-2}. The approximate tear energies of the particles, estimated in this way, are given in Table IV.

These tear energy values are of the order of magnitude of 100 J m^{-2}, and are thus similar to, if somewhat lower than, those in Table III, estimated from the composite toughness data. The lower tear energies in Table IV may be due to an underestimation of the value assumed for $\bar{G}$.

TABLE IV

Rubber	Composite	Γ_t (J m^{-2})
B	I	105–255
B	II	38– 83
C	II	98–158

Experimental errors or assumptions involved in calculating the tearing strains, λ^*, must also be considered (Equation 19). For example, the effective gauge length of the rubber particles may be less than the particle diameter. The difference between tear energies for particles of rubber B in types I and II composites (Tables III and IV) is attributed to variations in their chemical compositions resulting from the two fabrication methods. Nevertheless, the independent estimates of particle tear energies (Table IV) show tolerable agreement with those calculated from the toughness data of the composites themselves (Table III).

Typical energies of rubber are between 10^2 and 10^5 J m^{-2} [17, 18]; for example, those measured on bulk rubber samples, fabricated with similar compositions to the particles, ranged between 10^3 and 10^4 J m^{-2} [11]. Thus, a value of $\Gamma_t \approx 100$ J m^{-2} for the rubber particles (Tables III and IV) is comparatively low. Relative size (volume) and tearing rate of a rubber sample are important factors, however, in conventional measurements of Γ_t. For example, the energy dissipated in molecular flow or fracture, i.e. the tear energy, in a microscopic particle is expected to be significantly less than in a larger volume of rubber [11, 16]. The apparent tear energy of a particle will also be lower than that measured for bulk rubber if its effective strain (stretching) rate at the crack tip is lower than that used to test the bulk piece [11, 20].

The fact that the apparent tear energies in Table III are an order of magnitude smaller than typical bulk values suggests that the model overestimates the increase in toughness when conventional values of Γ_t for bulk rubber are substituted into Equation 15. Similarly, particulate tear energies, if they were available, would lead to an underestimation of the predicted toughening effect. The values of ΔG_{IC} generated in this study (Fig. 14) are notably low, however, compared to the order of magnitude increases in toughness obtained for other resin-hardener systems [8–10, 12, 21]. Performing a sample calculation to test the model, using McGarry, *et al.*'s data [8] of $G_{IC} \cong 4.4$ kJ m^{-2}, $G_{IC}^E \cong 0.3$ kJ m^{-2} and $V_P \cong 0.07$ in Equation 18 ($d < 1\,\mu$m; $\lambda_t > 4$), leads to $\Gamma_t \cong 14$ kJ m^{-2}. Similarly, using Scott and Phillips' data [21], where $G_{IC} \cong 3.2$ kJ m^{-2}, $G_{IC}^E \cong 0.33$ kJ m^{-2} and $V_P \cong 0.10$, gives a value for Γ_t of approximately 7 kJ m^{-2}. Both of these calculated tear energies are of the appropriate magnitude for

rubber, illustrating that, in general, the toughness increase of an epoxy–rubber composite can be predicted on the basis of the volume fraction and bulk tear energy of rubber.

5.4. Dependence of toughness on particle size

For a given rubber, the size of the particles tends to increase as the volume fraction of rubber (V_R) increases. Therefore, in order to distinguish between the effects of volume fraction and size of the particles on ΔG_{IC}, the latter is normalized with respect to V_P and plotted as a function of $\bar{d}$ in Fig. 15. The quantity $\Delta G_{IC}/V_P$ decreases by a factor of three for type II composites as the particle size increases from 0.1 to 10 μm, but remains relatively constant with $\bar{d}$ for type I material.

This behaviour can be compared with that predicted by the model in Equation 15. For the range of estimated values of Γ_t in Table IV, the ratio $\Delta G_{IC}/V_P$ does not vary significantly with λ_t when λ_t is greater than 4 which corresponds to particles smaller than of the order of 10 μm.

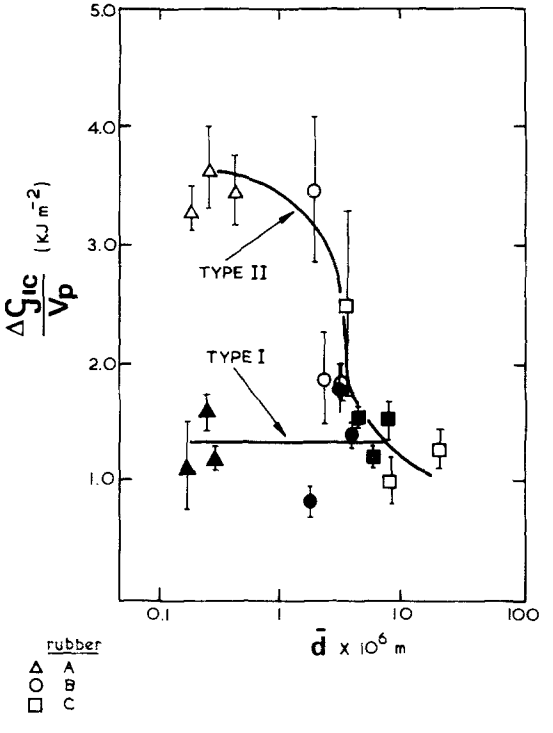

Figure 15 Normalized increase in toughness as a function of mean particle size for type I and type II epoxy–rubber composites.

When the particle size ($\bar{d}$) exceeds about 20 μm, the tearing strains fall to less than 4, and $\Delta G_{IC}/V_P$ decreases accordingly. Thus, Equation 15 predicts the toughening to be independent of $\bar{d}$ for the range of particle sizes investigated.

Fig. 15 shows that the results from type I composites agree with the predicted behaviour. In contrast, type II composites undergo a transition in $\Delta G_{IC}/V_P$ at particle sizes between 1 and 10 μm. This apparent size dependence can be related to a variation in the tearing energy of the different rubbers. Measurements of Γ_t from bulk samples of rubbers B and C (which correspond to the larger particle sizes) are between two and three times lower than those of rubber A [11]. This is consistent with the decrease in $\Delta G_{IC}/V_P$ at $d > 1$ μm. The tearing energies of particles in the type I composites do not appear to vary. This is attributed to their having a different chemical composition from those in the type II material due to the two methods of fabrication. The results in Fig. 15 support the theory that the toughening contribution of the particles depends primarily on the tearing energy of the rubber and only weakly on the particle size.

6. Discussion

6.1. Interpretation of toughness data

An explanation for the discrepancy between the toughness values generated in this study and those reported in the literature can be reached on the basis of chemical composition and cure schedule of the epoxy–rubber composites. It has been shown [22] that certain resin/hardener systems show a substantially smaller toughness increase with rubber particles present than others. This is attributed to the choice of hardener used to cross-link the resin and is thought to be due to differences in compatibility between the rubber and the resin/curing agent system. The hardener used in this study (DDM) is one of those shown to result in composites with a very low enhanced toughness. In contrast, those curing agents used by others [8, 12, 31] are known to yield markedly higher toughnesses.

The relatively high post-cure temperature (180° C) used in this study is expected to result in extensive cross-linking of both the matrix and the rubber–co-polymer particles; this would have the effect of reducing the stretching ability (λ_t, Γ_t) of the particles as well as limiting whatever ability exists for crazing or shear yielding of the surround-

ing matrix. Variations in both fabrication procedure (e.g. simple reaction versus pre-reaction) and cure cycle lead also to differences in particle morphology [11]; for example, the first factor affects the amount of occluded epoxy within the rubber which, in turn, is expected to directly influence critical toughening parameters such as λ_t and Γ_t of the particles.

Thus, in the resin/hardener system studied here, it is thought that the bulk tear energy of the rubber in the particles is in fact of the order of $100\,J\,m^{-2}$, a low value, resulting in a small ΔG_{IC}, due to the factors described above. Similarly, the toughness increases obtained by others follow from the resin/hardener systems used, and are consistent with the model's prediction, based on Γ_t of bulk rubber.

6.2. Comparison of model with other theories

In contrast to the model developed in this paper, other theories of toughening for epoxy–rubber composites ignore the contribution of the rubber particles themselves beyond their role as stress concentrators or as obstacles to craze growth. Crazing and shear yielding of the resin matrix, induced by the particles, are considered the dominant energy-absorbing processes (see, for example, [6, 9, 12]). It has been estimated that crazing can account for up to 55% of the fracture energy of a thermoplastic [23], thus, even if rubber particles do induce crazing in epoxy resin, the energy required would not be sufficient to entirely account for the observed increase in toughness. Results of an experiment designed to estimate the extent of craze-induced toughening showed that the toughness of an unmodified epoxy resin, containing approximately 6% by volume of spherical holes, did not differ significantly from that of the non-porous resin [11]. In contrast, a similar volume fraction of rubber particles, which in fact give rise to a smaller stress concentration than hollow voids, has a significant toughening effect. These observations argue for some other toughening mechanism(s) to include the deformation and properties of the rubber particles themselves.

With the exception of an isolated observation of what was interpreted as a craze [7], there is at present no conclusive evidence for this mechanism in epoxy–rubber composites. The possibility that the matrix contains some dissolved rubber which may prevent complete cross-linking of the resin and thus promote crazing has been postulated but not verified [21]. SEM fractographs examined in this study (for example, see Figs. 3 and 4) do not show voids or deformation in the matrix around the particle sites of the kind proposed by others [9, 10, 24]. Furthermore, the cavities left by the particles are lined with rubber which is consistent with a tearing process.

Shear band formation has also been proposed as a toughening mechanism on the basis of largely inconclusive fracture surface features [9, 10]. However, shear banding requires that the polymer strain softens after yielding; no significant yield drop was observed in stress–strain tests of pure epoxy resin nor of epoxy–rubber composites [11]. This suggests that the contribution of shear yielding to toughening may be of limited significance.

The most recent and comprehensive toughening theory [6] assumes that the rubber particles not only initiate crazing but also act as obstacles to craze growth. The particles reduce the inherent flaw size compared to that of an unmodified material such that a greater overall strain in the composite must be reached before fracture occurs. This leads to a higher craze density and high energy absorption. However, calculated critical flaw sizes of epoxy–rubber composites were found to be larger than that of the unmodified resin [11]. This means that instead of reducing the flaw size, the particles themselves become the strength-limiting flaws. Furthermore, a craze examined in an epoxy–rubber composite [7] was less than $1\,\mu m$ long whereas interparticle spacings are typically of the order of $10\,\mu m$ [11]. This makes it doubtful that rubber particles can play an important role as craze-stoppers unless the crazes are appreciably longer than observed.

7. Conclusions

Microscopic observations at the tip of a propagating crack reveal, in detail, the fracture mechanism of epoxy–rubber composites. Rubber particles which bridge the crack stretch to large strains before tearing and failing. A model for toughening is developed, based on the observations and on the concept that stored elastic energy in the particles is irreversibly dissipated during tearing. The model predicts that the tearing strain of a particle should increase as its size decreases; also, the contribution of the particles to the toughness should increase

with the volume fraction and tearing energy of the rubber, and be only weakly dependent on particle size. Detailed comparisons of experimental data with the model bear out these predictions.

Acknowledgements

One of us (S.K.D.) would like to thank Churchill College, Cambridge for financial support in the form of the Pochobradsky studentship. We are grateful to the B. F. Goodrich Chemical Company for generously donating the rubber. This work forms part of a larger research programme on Fracture of Polymers supported by the Science Research Council.

References

1. E. H. MERZ, G. C. CLAVER and M. BAER, *J. Polymer Sci.* **22** (1956) 325.
2. L. E. NIELSEN, "Mechanical Properties of Polymers" (Reinhold, New York, 1962).
3. J. A. SCHMITT and H. KESKKULA, *J. Appl. Polymer Sci.* **3** (1960) 132.
4. C. B. BUCKNALL and R. R. SMITH, *Polymer* **6** (1965) 437.
5. S. NEWMAN and S. STRELLA, *J. Appl. Polymer Sci.* **9** (1965) 2297.
6. C. B. BUCKNALL, "Toughened Plastics" (Applied Science, London, 1977).
7. C. B. BUCKNALL and T. YOSHII, Third International Conference on Deformation, Yield and Fracture of Polymers, PRI, Paper 13, Churchill College, Cambridge, April (1976).
8. F. J. McGARRY, A. M. WILLNER and J. N. SULTAN, Research Report R69-59, Massachusetts Institute of Technology (1969).
9. J. N. SULTAN, R. C. LIABLE and F. J. McGARRY, *Appl. Polymer Symp.* **16** (1971) 127.
10. R. DRAKE and A. SIEBERT, *SAMPE Quart.* **6** (1975).
11. S. C. KUNZ, Ph.D. Thesis, University of Cambridge (1978).
12. A. R. SIEBERT and C. K. RIEW, "The Chemistry of Rubber Toughened Epoxy Resins I", 161st American Chemical Society Meeting, Organic Coatings Plastic Division, Los Angeles, March (1971) p. 552.
13. S. VISCONTI and R. H. MARCHESSAULT, *Macromol.* **7** (1974) 913.
14. L. R. G. TRELOAR, "The Physics of Rubber Elasticity" (Oxford University Press, London, 1949).
15. E. E. UNDERWOOD, "Quantitative Microscopy", edited by R. T. DeHoff and F. N. Rhines (McGraw-Hill, New York, 1968) p. 149.
16. A. N. GENT, "Fracture", Vol. 7, edited by H. Liebowitz (Academic Press, New York, 1972) p. 315.
17. R. S. RIVLIN and A. G. THOMAS, *J. Polymer Sci.* **10** (1953) 291.
18. H. W. GREENSMITH and A. G. THOMAS, *ibid.* **18** (1955) 189.
19. H. M. JAMES and E. GUTH, *J. Chem. Phys.* **11** (1943) 455.
20. L. MULLINS, *Trans. Inst. Rubber Ind.* **32** (1956) 231.
21. J. M. SCOTT and D. C. PHILLIPS, *J. Mater. Sci.* **10** (1975) 551.
22. A. C. MEEKS, *Polymer* **15** (1974) 675.
23. R. P. KAMBOUR, *J. Polymer Sci. Macromol. Rev.* **7** (1973) 1.
24. W. D. BASCOM, R. L. COTTINGHAM, R. L. JONES and P. PEYSER, *J. Appl. Polymer Sci.* **19** (1975) 2545.

Received 21 February and accepted 13 September 1979.